


Structure, stability, and superconductivity of N-doped lutetium hydrides at kbar pressuresKaterina P. Hilleke¹,* Xiaoyu Wang,¹* Dongbao Luo, Nisha Geng, Busheng Wang¹, Francesco Belli, and Eva Zurek¹†
Department of Chemistry, State University of New York at Buffalo, Buffalo, New York 14260-3000, USA (Received 13 April 2023; accepted 16 June 2023; published 31 July 2023)

The structure of the material responsible for the room temperature and near ambient pressure superconductivity reported in an N-doped lutetium hydride [Nature (London) **615**, 244 (2023)] has not been conclusively determined. Herein, density functional theory calculations are performed in an attempt to uncover what it might be. Guided by a range of strategies including crystal structure prediction and modifications of existing structure types, we present an array of Lu-N-H phases that are dynamically stable at experimentally relevant pressures. Although none of the structures found are thermodynamically stable, and none are expected to remain superconducting above ~ 17 K at 10 kbar, a number of metallic compounds with fcc Lu lattices—as suggested by the experimental x-ray diffraction measurements of the majority phase—are identified. The system whose calculated equation of states matches best with that measured for the majority phase is fluorite-type LuH₂, whose 10 kbar superconducting critical temperature was estimated to be 0.1 K using the Allen-Dynes modified McMillan equation.

DOI: [10.1103/PhysRevB.108.014511](https://doi.org/10.1103/PhysRevB.108.014511)**I. INTRODUCTION**

Heike Kamerlingh Onnes' 1911 discovery of mercury's entrance into a "new...superconductive state" at very low temperatures, where all electrical resistance vanished [1], marked the beginning of a quest: could such a state be observed at room temperature? Ever since, scientists have sought this "holy grail," steadily breaking through barriers such as the boiling point of liquid nitrogen [2], 100 K [3], then near 200 K [4–6]. The latter breakthrough can be directly traced back to Ashcroft's proposal that hydrogen-rich alloys, metallized at conditions of extreme pressure, albeit less extreme than those required to metallize pure hydrogen, would be high-temperature phonon-mediated superconductors [7]. It also marked a paradigm shift defined by a close synergy between theory and experiment, with computations either predicting the most promising superconducting phases or being instrumental in characterizing compounds that had already been synthesized [8–10].

For the materials with the highest superconducting critical temperatures, T_c s, two things were true: they featured high hydrogen content and they required immense pressures—approaching those found in the center of the Earth (350 GPa)—for stability. One prominent class of these high-pressure high-temperature compounds is known as the "superhydrides." All of them are characterized by clathrate-like hydrogen-based lattices that encapsulate an electropositive metal atom, typically an alkaline or rare earth. Examples of compounds that have been both predicted and synthesized include CaH₆ ($T_c = 210$ – 215 K, 160–172 GPa) [11,12], LaH₁₀ ($T_c = 260$ K, 200 GPa) [13,14], YH₉ ($T_c = 262$ K, 182 GPa) [15], YH₆ ($T_c = 224$ K, 166 GPa) [16], and mixed La/Y ternary hydrides [17,18].

Clearly, the most prominent metal atoms in these phases are yttrium and lanthanum, with supporting roles played by calcium, scandium, and other rare earths. However, most of the heavier lanthanide hydrides are not expected to be as promising because of the suppressive influence of the f electrons on superconductivity, with maximum T_c s decreasing rapidly once past La [19,20]. As a result, the hydrides of lutetium received relatively little attention despite the fact that the filled $4f$ shell of the metal is chemically unreactive rendering its electronic properties similar to those of Sc, Y, and La, until now.

An early theoretical study generated a Lu-H convex hull using known polyhydride structures, finding LuH₄, LuH₆, LuH₉, and LuH₁₀ as being thermodynamically stable at various pressures up to 400 GPa [20]. Another identified a unique $Im\bar{m}m$ structure for LuH₈ with an estimated T_c of 81–86 K at 300 GPa, based on a distorted version of the backbone of the $Fm\bar{3}m$ LaH₁₀ phase [21]. A theoretical comparison between the hydrides of the rare-earth elements with filled versus unfilled f -states—Tm, Yb, and Lu—found LuH _{n} ($n = 4$ – 8 , 10) phases either on or very near the Lu-H convex hull at relatively low pressures (less than 200 GPa) [22]. Notably, LuH₆, with the same $Im\bar{3}m$ symmetry as CaH₆, had an estimated T_c of 273 K (matching the melting point of ice) at 100 GPa. The filled f -shells of Lu and Yb were suggested to confer a strong degree of phonon softening, thereby resulting in a high electron-phonon coupling. Finally, a theoretical investigation of trends in superconductivity proposed high-pressure Cc LuH₇ and $C222$ LuH₁₂ phases, with the latter predicted to undergo a superconducting transition below 6.7 K at 150 GPa [19]. On the experimental side, a recent work reported the synthesis of a Lu hydride, suggested to be $Pm\bar{3}n$ Lu₄H₂₃, with a measured T_c of 71 K at 218 GPa [23]. This structure has previously been observed in experimental studies in the La-H [24], Ba-H [25], and Eu-H [26] systems.

Thus, with reported T_c s of the superhydrides reaching temperatures not uncommon for a typical winter day in

*These authors contributed equally to this work.

†ezurek@buffalo.edu

upstate New York, the focus of research changed to predicting and synthesizing materials that could maintain high T_c s, but at lower pressures, with the ultimate goal of realizing superconductivity at ambient temperature and pressure. As the structures and superconducting properties of the binary hydrides had been exhaustively searched with no such candidate found, computations turned towards predicting ternary hydrides that remained dynamically stable to pressures below 100 GPa [27–29], or boron-carbon analogs of the superhydrides that were stable at 1 atm [30].

It was therefore quite exciting when a recent experimental manuscript reported superconductivity near room temperature, $T_c = 294$ K, at a very moderate pressure of 10 kbar (1 GPa) in a nitrogen-doped lutetium hydride phase [31]. This pressure is low enough so that it becomes feasible to use pressure-quenching [32] to stabilize the material to ambient conditions, or to use careful strain engineering to achieve the desired superconductivity. Unfortunately, though a variety of techniques including x-ray diffraction (XRD), energy-dispersive x-ray measurements, elemental analysis, and Raman spectroscopy were used to characterize the superconducting material, its composition and structure could not be fully resolved [31].

On the basis of the XRD and Raman analysis, the proposed room-temperature superconducting material (referred to as compound **A** by the authors) was indexed with space group $Fm\bar{3}m$, and both compound **A** and a minor product, which was dubbed compound **B**, were suggested to consist of an fcc Lu network with additional N and H uptake [31]. At pressures above ~ 30 kbar, the superconducting compound **A** was found to undergo a pressure-induced transition to a nonsuperconducting structure involving a symmetry reduction of the Lu lattice to orthorhombic $Immm$ symmetry.

The superconducting compound was also observed to undergo a sequence of color changes corresponding to structural transitions as pressure was applied, from blue to pink (marking the transition to the high- T_c superconductor) to red [31]. Follow-up studies have, however, suggested that this color change is derived in fact from pure LuH_2 [33–35], although it has also been observed in N-doped samples [36,37]. In some cases, the onset pressure for the color change was higher than that reported for the putative room-temperature superconductor. In one study, Raman and XRD measurements confirmed a trigonal to cubic transition under pressure for a Lu-N-H sample, and note low-frequency Raman modes that cannot be explained by pure cubic symmetry—similar to those observed in the superconducting compound and possibly arising from symmetry breaking N/H substitutions [38].

Experiments reported no evidence for superconductivity down to 1.5 K in LuH_2 [33], while another study found that the resistivity of LuH_2 is extremely sensitive to grinding processes [39]. Superconductivity was absent as well in measurements on $\text{LuH}_{2\pm x}\text{N}_y$ from ambient pressure to 6.3 GPa down to 10 K [34], and $\text{LuH}_{2\pm x}\text{N}_y$ up to 30 GPa down to 1.8 K [37]. The latter study also noted a resistance anomaly in warming cycles of both the reported superconducting phase and a nonsuperconducting phase above 200 K, which they suggest could be the source of a phantom superconducting transition [37]. Another study obtained fcc compounds with unit cells in line with the reported phases in

the room-temperature superconductor synthesis, but neither a superconducting transition nor a change from dark blue was observed in the resulting samples [40]. The electronic and magnetic properties of elemental Lu and LuH_2 [41] have also been studied.

Turning to computational studies: density functional theory (DFT) calculations concluded that LuH_2 in the fluorite structure is the dominant phase of the parent nitrogen-doped superconductor, based on its computed thermodynamic and dynamic stability, optical properties, and XRD pattern [42]. A computational exploration of the Lu-N-H phase diagram found no ternary phases on the convex hull at pressures below 10 GPa, with the binaries dominating instead, although a few ternary phases ($\text{Lu}_{20}\text{H}_2\text{N}_{17}$, $\text{Lu}_2\text{H}_2\text{N}$, LuH_5N_2 , $\text{Lu}_3\text{H}_6\text{N}$, and $\text{Lu}_{10}\text{HN}_8$) were within 100 meV/atom of the hull. A number of the identified phases were found to be derived from either H vacancies or N-doping of LuH_2 [43]. The $\text{Lu}_8\text{H}_{21}\text{N}$ phase, which lies 31 meV/atom above the 1 GPa convex hull, was constructed by partial N/H substitution, as well as the introduction of vacancies to eliminate too close H-H contacts [44]. Another computational study did not find any thermodynamically stable Lu-N-H phases at 1 GPa, and the highest T_c computed for N-doped $Fm\bar{3}m$ - LuH_3 did not exceed 30 K [45]. Indeed, estimates of superconductivity in all the studied binary and ternary phases in the Lu-N-H system are far too low to account for the reported superconducting properties [44,46,47]. The curious sequence of color changes has also been computationally investigated, with one study finding H-deficient LuH_2 as the best match to the experimental observations [48]. In short, a great deal of skepticism has been expressed [49] regarding the claim of room-temperature superconductivity in an N-doped LuH_3 -based phase.

Herein, we present a DFT investigation of a series of structures in the Lu-N-H system that were either constructed via modification of known and theoretical prototypes, via constrained and unconstrained crystal structure prediction (CSP) searches, or by a combination of these two methods. From the results of the unconstrained CSP runs, we obtain a baseline against which to measure the enthalpies of constructed phases and to compare their properties. From constrained searches and artificially constructed structures we begin to understand the motifs that contribute to dynamic stability at low pressures and those that do not, allowing us to narrow the range of possible structures for further explorations into the Lu-N-H ternary system. The simulated XRD patterns of the optimized phases and calculated equations of states are compared with available experimental data provided in Ref. [31]. The highest superconducting critical temperature we find—17 K at 10 kbar—was obtained for a CaF_2 -type LuNH phase that was far from thermodynamic stability.

II. COMPUTATIONAL DETAILS

Precise geometry optimizations and electronic structure calculations were performed using DFT in conjunction with the Perdew-Burke-Ernzerhof (PBE) functional [50], as implemented in the Vienna *ab initio* simulation package (VASP) [51–53]. The valence electrons of the hydrogen ($1s^1$), nitrogen ($2s^2 2p^3$), and lutetium ($5p^6 5d^1 6s^2$) atoms were simulated using plane-wave basis sets with a cutoff energy

of 600 eV. The core electrons were treated with the projector augmented wave (PAW) method [54]. Detailed tests of the inclusion of the $4f$ electrons on the properties of select structures, as well as the convergence of the plane-wave basis, were performed, and representative results are provided in the Supplemental Material [55]. The reciprocal space was sampled using a Γ -centered Monkhorst-Pack mesh [56], where the number of divisions along each reciprocal-lattice vector was chosen such that the product of this number with the real-space lattice constant was 70 Å for density of states calculations and 50 Å for static calculations. To interrogate the dynamic stability of promising phases, phonon calculations were performed using the finite-difference scheme, as implemented in the PHONOPY software package [57,58].

In contrast to various lanthanide hydrides where the f states are partially filled and where it was recently shown that strong correlations affect the computed T_c [59], our Lu-N-H results are in line with previous theoretical studies that found the f bands in high-pressure LuH₆ to be below the Fermi level, and therefore likely not involved in the superconducting mechanism [22]. Likewise, computations on the color changes in LuH₂ [48] found only a minor influence from correlation effects in Lu, testing both the Hubbard U parameter and dynamical mean-field theory calculations. In that study, it was noted that the large dispersion of the Lu $5d$ states likely minimizes the importance of local correlation effects.

Herein, the electron-phonon coupling (EPC) calculations were performed using the QUANTUM ESPRESSO (QE) package [60,61] version 7.1 with the PBE functional. A plane-wave basis set with a cutoff energy of 80 Ry was used, along with a charge-density cutoff of 640 Ry for the valence electrons of hydrogen (H $1s^1$), nitrogen (N $2s^2 2p^3$), and lutetium (Lu $5s^2 5p^6 6s^2 5d^1$). The core electrons were treated with the PAW potentials generated using the PSLIBRARY package [62]. The k -point and q -point grids were selected to ensure that the total EPC constant, λ , was converged to within 0.05 at the desired Gaussian broadening width for each structure, as summarized in the Supplemental Material [55].

The superconducting critical temperature (T_c) was estimated using the Allen-Dynes modified McMillan equation [63]:

$$T_c = \frac{\omega_m}{1.20} \exp \left[-\frac{1.04(1 + \lambda)}{\lambda - \mu^*(1 + 0.62\lambda)} \right], \quad (1)$$

in which the effective Coulomb potential, μ^* , was set to 0.1, the logarithmic average frequency ω_m was obtained by

$$\omega_m = \exp \left(\frac{2}{\lambda} \int \frac{d\omega}{\omega} \alpha^2 F(\omega) \ln \omega \right), \quad (2)$$

and the EPC constant, λ , was evaluated by

$$\lambda = \int d\omega \alpha^2 F(\omega) / \omega. \quad (3)$$

The Eliashberg spectral function, $\alpha^2 F(\omega)$, was obtained from the QE calculations, and was also used to numerically solve the Eliashberg equations [64].

The CSP searches were performed using the open-source evolutionary algorithm (EA) XTALOPT [65–67] version 12 [68]. The initial generation consisted of random symmetric structures created by the RANDSPG algorithm [69]. Duplicate

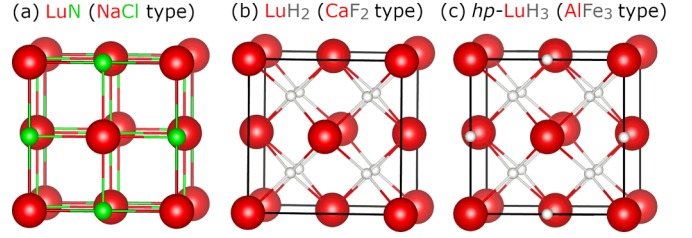


FIG. 1. Prototype Lu-N and Lu-H structures with fcc Lu lattices: (a) NaCl-type LuN, (b) CaF₂-type LuH₂, and (c) a high-pressure (hp) phase of LuH₃.

structures were identified via the XTALCOMP algorithm [70] and discarded from the breeding pool. Constrained XTALOPT searches were performed by determining the symmetry of the Lu atoms using Pymatgen [71] and only keeping those structures in the breeding pool that possessed an $Fm\bar{3}m$ symmetry Lu sublattice [72]. The parameters employed in the XTALOPT searches for the considered stoichiometries (number of formula units, pressures at which the EA searches were performed, and constraints employed) are provided in the Supplemental Material [55].

III. RESULTS

A. Known ambient pressure phases

Before we begin our theoretical investigation of novel Lu-N-H combinations that could be formed at mild pressures, let us review the structures and properties of the known LuH_x and LuN phases. Unlike the high-pressure superhydrides, which bear little to no resemblance to the hydrides that are known at ambient conditions, the 1 atm LuN and LuH_x phases may provide the key to the structure of Lu-N-H—or at least very good starting points—stemming from the relatively low pressures required to stabilize this ternary phase as suggested by recent experiments [31].

At ambient pressure, LuN assumes the rocksalt, or $B1$, structure [Fig. 1(a)], with the Lu atoms in the fcc configuration. A transition to the $B2$ or CsCl phase has been predicted near 250 GPa [73]. Our PBE calculations, which likely underestimate the band gap, suggest semiconducting behavior at 1 atm with a gap of 0.23 eV. In compounds, lutetium typically adopts the +3 oxidation state, and its hydrides can incorporate vacancies or extra hydrogen atoms that go into the interstitial regions [74]. At 1 atm, fluorite (CaF₂-type) LuH_x is adopted when $x = 1.85$ – 2.23 [Fig. 1(b)], usually resulting in a metallic phase. Increasing the hydrogen content to $x = 2.78$ – 3 yields a hexagonal semiconducting phase [74]. This $P\bar{3}c1$ LuH₃ transitions to a cubic phase at ~ 10 GPa [the AlFe₃ or $D0_3$ structure type, Fig. 1(c)], which can be stabilized at ambient via milling [75]. Recently, superconductivity in $Fm\bar{3}m$ -LuH₃ was reported with a T_c of 12.4 K at 122 GPa [76].

To validate the computational settings used in this study, we compared the lattice constants of the known phases where the Lu atoms are found in the fcc arrangement: rocksalt LuN (4.760 Å [77]) and fluorite-type LuH₂ (5.033 Å [78]) with those of the optimized structures. The DFT lattice constants differed by only 0.17% and 0.28% from experiment,

further supporting the choice of our computational parameters. These known ambient-pressure nitrides and hydrides of lutetium provide a basis that could be used to build models of the high- T_c superconducting phase reported in Ref. [31]. In fact, the similarity of the 1 atm lattice parameters of phase **A** [5.0289(4) Å] and the (presumably nonsuperconducting) compound **B** (4.7529 Å) with the known dihydride and nitride of lutetium, respectively, coupled with a comparison of the DFT-optimized unit-cell parameters of several hypothetical and selected partially doped versions of the known compounds, were used to assign possible compositions [31]. Phase **A** was tentatively assigned as $\text{LuH}_{3-\delta}\text{N}_\epsilon$, with partial N substitution onto H sites in the cubic (high-pressure) LuH_3 , and phase **B** as $\text{LuN}_{1-\delta}\text{H}_\epsilon$, an H-doped variant of rocksalt LuN [31]. On the other hand, a recent theoretical manuscript proposed that CaF_2 -type LuH_2 is the parent structure of the superconducting phase, and compound **B** could be the rocksalt LuH structure, which is dynamically stable at 0 GPa [42].

B. Newly predicted phases

The structures investigated herein were generated using a variety of procedures including *ab initio* CSP techniques, as well as modification of known phases and compounds predicted using CSP. The advantage of CSP searches is that they can, freed from structural preconceptions, locate the low-lying configurations in a potential energy surface, whose complexity here is heightened by the inclusion of three elements. Such searches can be unconstrained, purely hunting down the lowest-enthalpy configurations given a certain stoichiometry. Constraining a search to structures containing a particular motif will narrow down the possible results, but could also miss out on even lower-enthalpy alternatives that do not align with the constraints.

To that end, a combination of both unconstrained and constrained CSP searches was carried out for the Lu-N-H system using the XTALOPT EA. From the former, we can learn about the structural motifs that yield the most stability, and comparison with the latter informs us of the enthalpic cost associated with a specific structural feature. In addition, various structures were made “by hand” via modification of known prototypes or CSP-generated structures that possess an fcc Lu lattice. As we will soon see, a large structural variety is present among the dynamically stable phases that we found, highlighting the difficulties inherent in the computational prediction of metastable phases that could potentially be synthesized.

1. Semiconductors

Unconstrained XTALOPT searches for the lowest-enthalpy structures were performed for the $\text{Lu}_3\text{NH}_{11}$, $\text{Lu}_4\text{NH}_{10}$, and $\text{Lu}_4\text{NH}_{11}$ compositions at both 0 and 3 GPa, as well as for Lu_4NH_6 and LuNH_2 at 0 GPa. These EA runs located a number of structurally diverse semiconducting phases with PBE band gaps that ranged from 1.1 to 2.1 eV; some are shown in Fig. 2. A few of the predicted structures, including $P2_1m$ LuNH_2 and two $\text{Lu}_3\text{NH}_{11}$ phases—one with $P1$ symmetry at 0 GPa and one with Cm symmetry at 3 GPa—possessed large empty regions. $P2_1m$ LuNH_2 [Fig. 2(a)] is, in fact, a fully 2D compound. At 0 GPa, Pc $\text{Lu}_4\text{NH}_{11}$ [Fig. 2(b)] was also

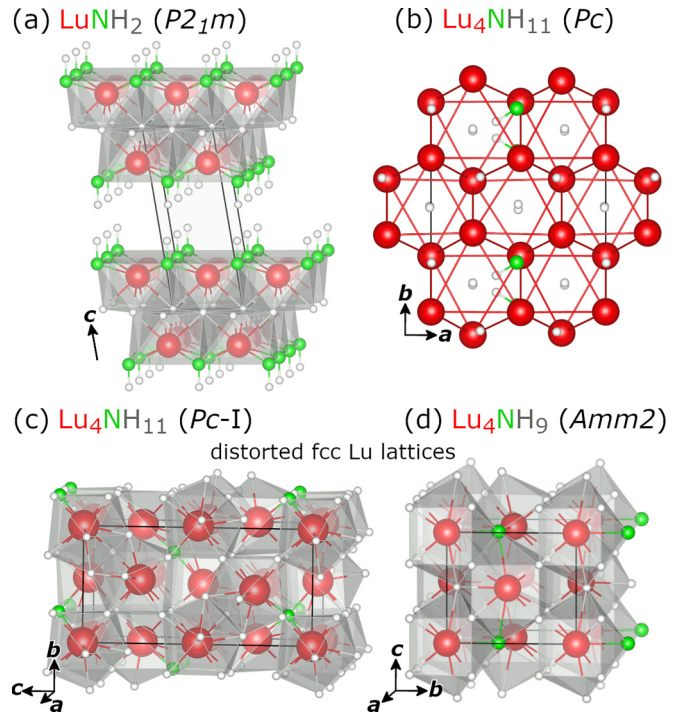


FIG. 2. Semiconducting Lu-N-H phases found using unconstrained evolutionary crystal structure searches [(a)–(c)] and prototype modification (d).

identified; it consists of layers of trigonal nets of Lu with H atoms in the resulting hexagonal channels, while the N atoms are arranged in zigzag chains oriented along the c -axis that weave into the Lu network (into the plane of the page).

Two of the structures from unconstrained searches— $P1$ $\text{Lu}_4\text{NH}_{10}$ (at 0 GPa) and a second Pc $\text{Lu}_4\text{NH}_{11}$ structure [at 3 GPa; Fig. 2(c)]—possessed Lu sublattices in slightly distorted fcc arrangements. In $P1$ $\text{Lu}_4\text{NH}_{10}$, the N atoms go into some of the sites octahedrally coordinated by Lu, while some H atoms go into the tetrahedral interstices and the rest are scattered across the unit cell, resulting in the very low symmetry. For Pc -I $\text{Lu}_4\text{NH}_{11}$ [Fig. 2(c)], the N atoms go instead into the tetrahedral interstices, and the hydrogen atoms take the octahedral and most of the remaining tetrahedral interstices. The fcc Lu lattice is also preserved in a semiconducting $Amm2$ compound with Lu_4NH_9 stoichiometry [Fig. 2(d)], which was produced not by CSP but by modifying the geometry of the high-pressure AlFe_3 -type LuH_3 compound. Here, H again partially occupies both tetrahedral and octahedral interstices in fcc Lu, leaving 1/4 of the tetrahedral interstices empty with 1/4 of the H atoms filling octahedral interstices being replaced by N.

From these results, it is clear that a variety of geometric motifs can be found in the low-enthalpy Lu-N-H compounds, highlighting both the difficulty of honing in on a single structure and the utility of guidance from experimental data. The unit cell volumes of several of the systems identified via unconstrained CSP searches were too large for them to stay as candidates for the putative superconducting phase. Importantly, because all of the aforementioned compounds were semiconducting, it is impossible for any of them to be

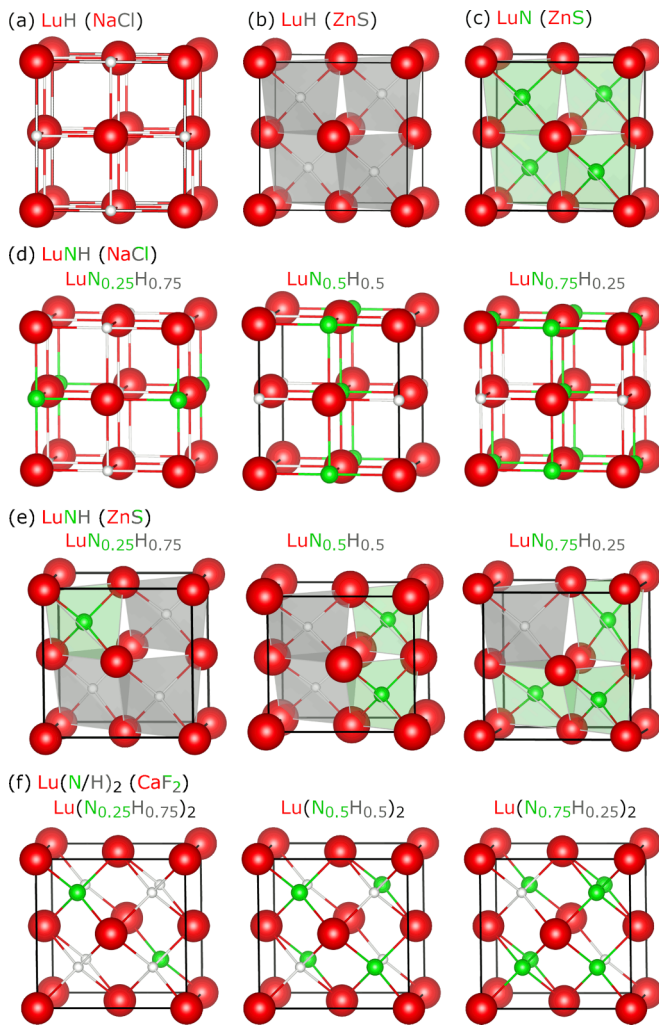


FIG. 3. Illustrations of hypothetical (a) rocksalt ($B1$) LuH, and zinc-blende ($B3$) LuH and (c) LuN phases. (d) Rocksalt and (e) zinc-blende $\text{LuN}_x\text{H}_{(1-x)}$, and (f) fluorite ($C1$) $\text{Lu}(\text{N}_x\text{H}_{(1-x)})_2$ solid solution models that were considered.

superconductors. Our search continues, with inspiration taken from known experimental phases or CSP searches guided via constraints toward desired structural features—or both.

2. Structures from prototype modification

The relatively low pressures needed to stabilize the putative room-temperature superconducting phase highlight the importance of—and inspiration to be gleaned from—examining the ambient- and low-pressure compounds formed between Lu and either N or H. Notably, within most of these, the Lu atoms adopt the fcc arrangement that has been suggested for the superconducting phase.

In addition to the ambient pressure $B1$ mononitride, LuN [Fig. 1(a)], we considered a hypothetical rocksalt monohydride, LuH [Fig. 3(a)], and hypothetical zinc-blende (or $B3$) LuN and LuH phases [Figs. 3(b) and 3(c)]. To explore the potential of a solid solution between the two rocksalt phases, calculations were carried out on the unit cells shown in Fig. 3(d). From these, only $\text{LuN}_{0.25}\text{H}_{0.75}$ and $\text{LuN}_{0.5}\text{H}_{0.5}$ were dynamically stable at 0 GPa. Similarly, solid solutions of

zinc-blende LuN and LuH were optimized [Fig. 3(e)], and from these LuH, $\text{LuN}_{0.5}\text{H}_{0.5}$, $\text{LuN}_{0.75}\text{H}_{0.25}$, and LuN were 0 GPa dynamically stable.

N/H substitution into the fluorite-type, or $C1$, LuH₂ phase [Fig. 1(b)] yielded another set of potential candidates [Fig. 3(f)], with $\text{LuN}_{0.5}\text{H}_{1.5}$ and LuNH being dynamically stable at 0 GPa. LuNH is a half-Heusler-like compound with equal amounts of N and H occupying the tetrahedral interstices of the Lu lattice. From the dynamically stable phases identified in this section, $C1$ $\text{LuN}_{0.5}\text{H}_{1.5}$ is weakly metallic under PBE-DFT, and thus likely in actuality it is a nonmetal. The rest are metallic. Below, we will compare the pressure-volume relations calculated for the phases discussed in this section with the experimental results obtained for compounds A and B, and we discuss the thermodynamic stability, electronic structure, and potential for superconductivity in these prototype-based Lu-N-H phases.

3. Structures inspired by evolutionary searches

Figure 4 illustrates a number of 0 GPa dynamically stable, metallic phases with fcc Lu sublattices that were found in a variety of ways. The $Fd\bar{3}m$ Lu₄NH₇ phase [Fig. 4(a)] was found in an unconstrained evolutionary search performed at 1 GPa. It can be constructed from a modified $2 \times 2 \times 2$ supercell of CaF₂-type LuH₂, in which 1/8 of the tetrahedral interstices of the Lu lattice are occupied by N rather than H. The distribution of the N atoms throughout the unit cell is in a diamondlike lattice. In this structure, the octahedral interstices of the Lu lattice are left empty. This structure belongs to the same family of phases illustrated in Fig. 3(f), representing another N-substituted CaF₂-type LuH₂ derivative. However, rather than being derived from prototype modification, it was located in an XTALOPT search and then served as a template to construct additional metastable phases. One of these, $Fd\bar{3}m$ Lu₂NH₅ [Fig. 4(b)], was generated by placing H₂ units into some of the empty octahedral interstices of the Lu lattice, and replacing an additional H atom from Lu₄NH₇ by N, so that the N atoms now trace out a bcc network within the structure, leaving H₂ molecules lying along only half of the N-N contacts.

Another (incomplete, or prematurely terminated) XTALOPT search at 1 GPa identified $P\bar{4}3m$ Lu₄NH₆ [Fig. 4(c)], which was chosen for further analysis and modification due to its dynamic stability, and the good match between its simulated XRD pattern with experiment. Like $Fd\bar{3}m$ Lu₄NH₇, $P\bar{4}3m$ Lu₄NH₆ is similarly a variant of the CaF₂-type LuH₂ structure, in which 1/8 of the tetrahedral interstices of the Lu lattice are occupied by N rather than H, and an additional 1/8 of the tetrahedral interstices are left empty. Rather than the diamondlike distribution of N atoms found in Lu₄NH₇, the substituting N atoms and vacancies are arranged in a CsCl-type framework. Filling the vacancies in Lu₄NH₆ with N atoms yields the $Pn\bar{3}m$ Lu₂NH₃ structure [Fig. 4(d)].

In most of the above phases, N atoms were positioned in the tetrahedral interstices of an fcc Lu framework, whereas in Lu₂NH₅ the octahedral interstices were partially occupied by H₂ molecular units. In $R\bar{3}m$ Lu₄NH₄, which was identified using an XTALOPT search carried out at 6 GPa where the Lu sublattice was constrained to maintain the $Fm\bar{3}m$ space group,

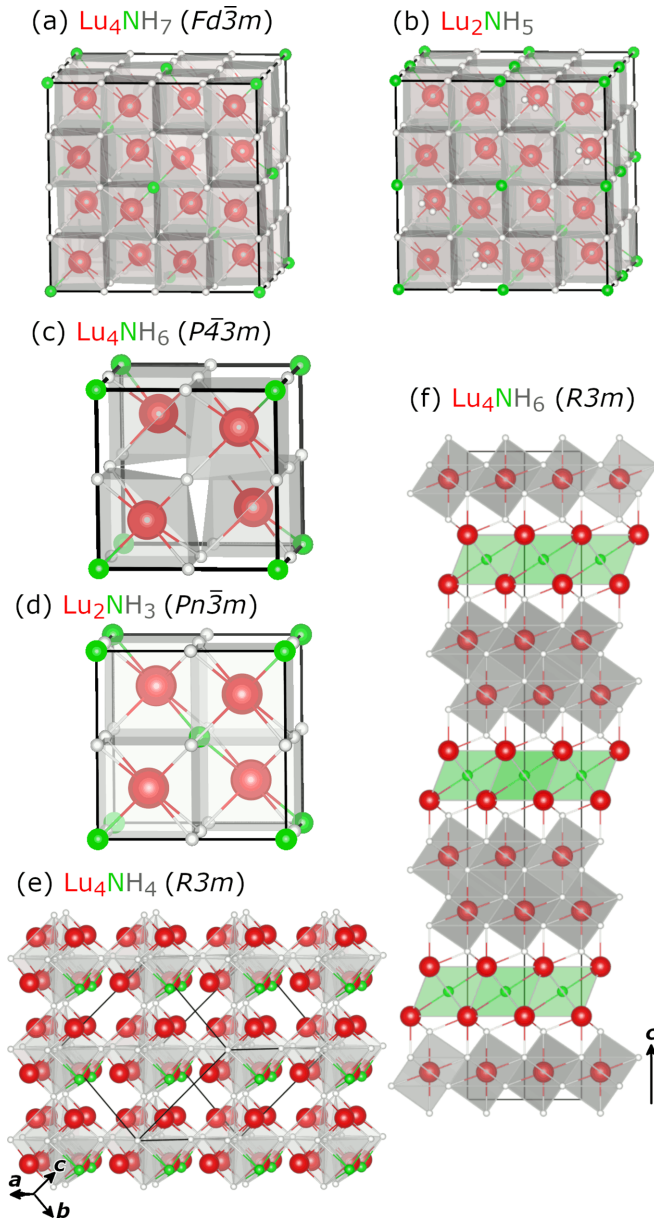


FIG. 4. Crystal structures of various dynamically stable Lu-N-H phases obtained from a combination of CSP searches—some constrained—and subsequent modification. Lu_2NH_5 and Lu_2NH_3 had PBE band gaps of 1.09 and 0.06 eV at 10 kbar.

the N atoms are not found within the tetrahedral holes but instead lie on 1/4 of the octahedral holes of the Lu lattice [Fig. 4(e)]. The N atoms in Lu_4NH_4 trace out a simple cubic arrangement, with their positions shifted slightly off of the center of the surrounding Lu_6 octahedra, while the tetrahedral interstices are half occupied by H and half are left empty. The remaining H atoms can be grouped into H@H_6 vertex-sharing octahedra.

The unconstrained 0 GPa XTALOPT searches that mainly uncovered the semiconducting compounds shown in Fig. 2 also produced the metallic $R3m$ Lu_4NH_6 phase [Fig. 4(f)]. In this phase, the Lu-N and Lu-H interactions become separated, with layers of N@Lu_6 octahedra—in essence, slabs of $B1$ LuN—interrupting a CaF_2 -type packing of Lu and

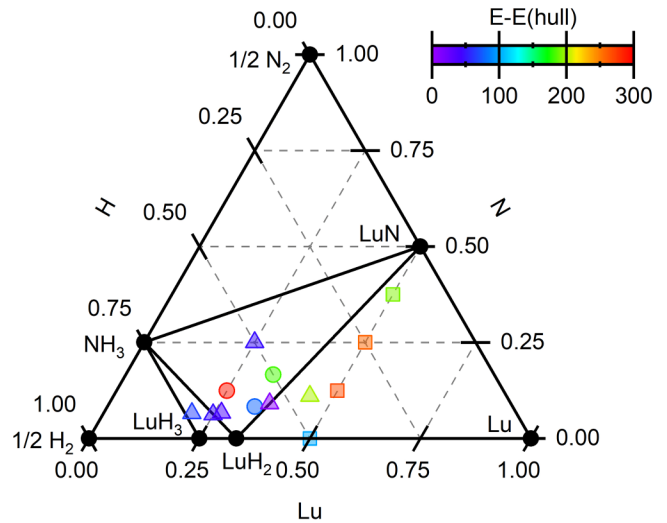


FIG. 5. Convex hull at 0 GPa. Only dynamically stable structures within 300 meV/atom above the hull are shown. If multiple structures exist for the same stoichiometry, only the most stable structure is listed. Black dots represent thermodynamically stable phases on the hull, and the colored points are colored by their distance from the hull in meV/atom. Triangles: structures generated via evolutionary search. Boxes: structures from prototype modification. Circles: structures generated by inserting atoms into structures derived from EA searches.

H. Because this phase was found using an EA search that generated sufficient structures to explore the potential energy landscape, it was 136.1 meV/atom lower in enthalpy than the previously discussed $P43m$ Lu_4NH_6 , and at 5 GPa this difference increased to 175 meV/atom. Perhaps this structure, with N-rich layers intercalated into a LuH_2 matrix, could hint at a strategy for inducing epitaxial strain on simple LuH_n structures, thereby altering their electronic and mechanical properties from those of their parent.

IV. PROPERTIES: STABILITY, EQUATION OF STATE, ELECTRONIC STRUCTURE, SUPERCONDUCTIVITY

A. Thermodynamics

The thermodynamic stability of the new structures was investigated by calculating their formation enthalpies relative to the solid elemental phases as a function of pressure. The reference phases employed were Lu: α -Sm (0–8 GPa [79]) and the hexagonal phase (9–10 GPa [80]); H_2 : $P6_3/m$ phase (0–10 GPa [81]); and N_2 : α - N_2 phase (0–7 GPa [82]) and ϵ - N_2 phase (8–10 GPa [83]). Known experimental phases including fluorite-type LuH_2 , $B1$ LuN, $P\bar{3}c1$ LuH_3 , and $P2_13$ NH_3 [84] were also considered.

The 0 GPa convex hull shown in Fig. 5 illustrates that only the known structures are thermodynamically stable, and all of the previously discussed Lu-N-H compounds are thermodynamically unstable within the static lattice approximation. Up to 10 GPa, only the known phases lie on the hull, while all others lie above it. A structure's thermodynamic stability can be characterized by its distance to the convex hull, which is plotted as a function of pressure (for all compounds, regardless of their dynamic stability). Herein, we employ

70 meV/atom, which corresponds to the 90th percentile of the DFT-calculated metastability of all of the known inorganic crystalline materials [85], as a gauge to identify those structures that could potentially be synthesized. At 0 GPa only five structures—all found using our unconstrained crystal structure search—fall in this range. From these only $R3m$ Lu_4NH_6 was metallic.

Let us now turn to the metallic phases with fcc Lu lattices. For the rocksalt solid-solution family, hydrogen concentrations ranging from 25% to 100% were roughly within 150–250 meV/atom from the hull, with $B1$ LuH as the lower boundary. For the zinc-blende solid-solution system this range expanded to 100–500 meV/atom, with $B3$ LuH corresponding to the lower boundary as well. Doping fluorite LuH_2 causes its energy to explode quickly: 25% nitrogen content results in an increase of energy by ~ 200 meV/atom above the convex hull, which rises to ~ 550 meV/atom for a 50% composition, and 1.1 eV/atom for 75% nitrogen content. The 0 GPa ternary convex hull plot shows that most of the low-enthalpy metastable structures are found at the bottom left-hand corner. The reason for this is that these are the only regions where full unconstrained CSP searches were performed, and the survivor bias makes us think that this region is where stable structures might appear. It should be noted, however, that these stoichiometries were chosen because exploratory calculations suggested their volumes were likely to provide the best match with the experimental equation of states of compound **A**. This will be explored shortly below.

Assuming linear behavior of the enthalpy-pressure relation, we were able to estimate the pressure where the considered phases may become thermodynamically stable if the slope of the distance from the hull versus pressure is negative. This estimate does not take into account the dynamic stability, nor does it include temperature or effects arising from the zero-point motion of the nuclei. The results suggest that $B1$ LuN-LuH mixtures become favored at high-pressures: LuH by ~ 30 GPa, ~ 50 GPa for $\text{LuN}_{0.25}\text{H}_{0.75}$, about 70 GPa for $\text{LuN}_{0.5}\text{H}_{0.5}$, and 80 GPa for $\text{LuN}_{0.75}\text{H}_{0.25}$. The higher the hydrogen concentration, the lower the predicted stabilization pressure, with a lower boundary of 30 GPa for $B1$ LuH. The slope of the other two solid solutions considered, $B3$ - and $C1$ -type, is positive, suggesting that they will never be stabilized. Two further phases that could potentially be stabilized within the megabar range are $R3m$ Lu_4NH_6 (16 GPa) and P_1 $\text{Lu}_4\text{NH}_{10}$ (34 GPa) because they are very close to the hull. The rest of the structures either possess a positive slope, or they cannot be stabilized until at least 140 GPa.

B. Equations of state and x-ray diffraction patterns

One of the key experimental observables guiding our choice of stoichiometries was the pressure-volume relation, or equation of state (EOS), of the majority phase presented in Ref. [31], which was assigned tentatively as an $Fm\bar{3}m$ structure with a $\text{LuH}_{3-\delta}\text{N}_\epsilon$ stoichiometry (or compound **A**). Above ~ 30 kbar, a first-order structural phase transition with a $\sim 0.3\%$ volume discontinuity was observed suggesting that the metal lattice of the resulting nonsuperconducting phase distorted to the $Immm$ spacegroup. In Fig. 6 we plot the EOS fits from Ref. [31] for the majority phase, which were

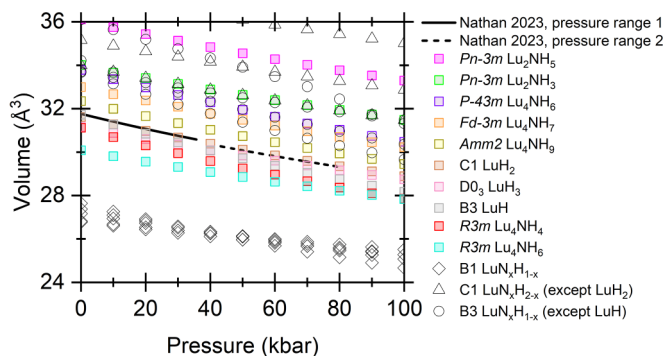


FIG. 6. The DFT calculated pressure-volume relationship or equation of states (EOS) of the Lu-N-H phases considered in this study. The colored squares correspond to the specified structures, and the open diamond, triangle, and circles correspond to various structures comprising the $B1$, $B3$, and $C1$ solid solution series (see Fig. 3), except for $C1$ LuH_2 and $B3$ LuH. The black lines represent the EOS fitted using the Birch-Murnaghan method for compound **A** using data from the pressure ranges $0 < P < 40$ kbar (solid) and $P > 42.7$ kbar (dashed) [31].

obtained for two pressure ranges. Choosing stoichiometries whose volumes matched well with experiment was initially nonintuitive because the effective radius of the metal atom changes substantially with its oxidation state being largest for Lu and smallest for Lu^{3+} .

From all of the phases we considered, both fluorite LuH_2 and zinc-blende LuH presented the best match with the experimental data below 40 kbar. At higher pressures, however, the volume of $B3$ LuH was computed to become progressively smaller than the measured value for compound **A**. The good agreement with $C1$ LuH_2 , on the other hand, remained up to at least 80 GPa. At 0 GPa, $B3$ LuH was slightly larger than $C1$ LuH_2 , in line with the general notion that the effective radius of Lu^+ is larger than that of Lu^{2+} . However, the volume of $B3$ LuH shrinks much faster (with a slope that is similar to that of $B1$ LuH) with increasing pressure as compared to that of $C1$ LuH_2 , while the volume of cubic LuH_3 shrinks at an even slower rate. Thus, the compressibility in these compounds appears to be dependent upon the repulsion exhibited between the ionic cores, with a larger number of H^- anions resulting in a higher resistance to compression. Due to its larger ionic radius, N^{3-} is less compressible than H^- . Since the computed EOS of cubic LuH_3 has a smaller slope than the EOS derived from experiment, and introduction of nitrogen will decrease the slope further, it could be expected that a compound with the $\text{LuH}_{3-\delta}\text{N}_\epsilon$ stoichiometry that was proposed for compound **A** would not have a slope that coincides with the experimentally derived EOS, unless potential vacancies play a substantial role.

In addition to the variety of structures discussed above, we also used the AFLOW-POCC module [86], used to generate models of off-stoichiometry phases, to produce an exhaustive array of structures based on partial N substitution for H in AlFe_3 -type LuH_3 , including supercells. This resulted in seven structures with $\text{Lu}_4\text{NH}_{11}$ stoichiometry, none of which were dynamically stable, and 113 structures of $\text{Lu}_{10}\text{N}_3\text{H}_{27}$ stoichiometry. 103 of these were eliminated from further study

due to their unit-cell volumes being too large to fit the measured value for compound **A**, greater than 32 \AA^3 , and the remaining 10 were also found to be dynamically unstable. More complex stoichiometries, potentially including vacancies as well as N/H substitution, cause the number of potential structures to balloon rapidly, beyond the scope of this study.

Because the calculated EOS of fluorite LuH_2 across the whole pressure range yielded the best fit with the experimentally reported EOS, we employed the quasiharmonic approximation to obtain a temperature-dependent EOS. Fitting the resulting EOS using the Birch-Murnaghan method at 300 K yielded V_0 (reference volume at $P = 0$) of 31.85 \AA^3 , K_0 (bulk modulus at $P = 0$) of 922.8 kbar, and K'_0 (dK_0/dP at $P = 0$, dimensionless) of 3.7. Setting K'_0 to 4, the EOS fit at 0 K yielded $K_0 = 928.8$ kbar and $V_0 = 31.61 \text{ \AA}^3$ [87]. This compares well with the values presented in Ref. [31] obtained using fits to data collected below (above) 40 kbar of 31.74 (31.6) \AA^3 , 886.4 (900) kbar, and 4, respectively.

To determine if the structures discussed here could yield XRD patterns similar to those observed in experiment, their simulated 0 GPa XRD patterns were generated, as was an XRD pattern for a model $Fm\bar{3}m$ Lu cell whose lattice constant ($a = 5.029 \text{ \AA}$) was in line with the refined unit cell suggested for superconducting compound **A** at 0 GPa (plots are provided in the Supplemental Material [55]). The PYXTAL XRD Similarity tool [88] was used to assess the similarity between the simulated powder XRD patterns of the proposed structures and that of the model $Fm\bar{3}m$ Lu cell, with a value of 1 corresponding to a perfect match and 0 to no match at all. The strongest matches came from the experimental phases CaF_2 -type LuH_2 (0.9848), AlFe_3 -type LuH_3 (0.9316), and from ZnS -type LuH (0.9962)—in line with the volume of $B3$ LuH adhering closely to the experimental EOS near 0 GPa. Of the N/H-doped NaCl , ZnS , and CaF_2 -type structures, the best XRD matches could be attributed to the ZnS -based phases, with the NaCl -based phases comparing most poorly. Of the phases directly obtained from XTALOPT searches or based on modifications of XTALOPT results, $Fd\bar{3}m$ Lu_4NH_7 and $R3m$ Lu_4NH_4 provided the best matches, although their enthalpies place them well above the convex hull in the pressure range of interest.

C. Electronic structure and superconductivity

Superconductivity has been measured in elemental Lu at pressures above ~ 100 kbar, with T_c rising to ~ 0.6 K near 160 kbar [89]. Adding hydrogen and mild pressure does not improve the superconducting properties much or at all: superconductivity in LuH_2 was not observed down to 1.5 K at pressures as high as 7.7 GPa [33]. These recent experimental results are in agreement with our computed values at 10 kbar, obtained via the Allen-Dynes modified McMillan equation, which is thought to be appropriate for phonon-mediated superconductors whose $\lambda < \sim 1-1.5$. As shown in Table I, we found that the T_c of fluorite-type LuH_2 was ~ 0.1 K, due to a small ω_{ln} combined with a modest $\lambda = 0.29$. Calculations on $Fm\bar{3}m$ - LuH_3 at 120 GPa yielded $\lambda = 0.30$ and $\omega_{ln} = 828$ K, resulting in $T_c = 0.36$ K, which is significantly smaller than the reported value of 12 K at 120 GPa [76].

TABLE I. The electron phonon coupling, λ , logarithmic average frequency, ω_{ln} , and superconducting critical temperature, T_c , estimated using the Allen-Dynes modified McMillan equation with $\mu^* = 0.1$ at 10 kbar for select Lu-N-H compounds. For LuNH the numerical solution of the Eliashberg equations was employed to obtain the value in parentheses.

Structure	λ	ω_{ln} (K)	T_c (K)
CaF_2 -type LuH_2	0.29	302	0.1
CaF_2 -type LuNH	0.78	377	16.9 (18.3)
CaF_2 -type $\text{LuN}_{0.5}\text{H}_{1.5}$	0.11	680	0.0
$R3m$ Lu_4NH_4	0.64	151	4.2
$P43m$ Lu_4NH_6	0.48	291	2.9
$Fd\bar{3}m$ Lu_4NH_7	0.47	435	4.2
$R3m$ Lu_4NH_6	0.29	306	0.1

To study the potential for superconductivity in ternary Lu-N-H compounds, we performed EPC calculations for the previously discussed metallic phases that were dynamically stable at 10 kbar—the pressure at which the maximum T_c was observed in Ref. [31]. Table I shows that though the T_c s of most of these phases (with the exception of $\text{LuN}_{0.5}\text{H}_{1.5}$) were predicted to surpass that of $C1$ LuH_2 , they do not even reach the boiling point of liquid nitrogen, in agreement with recent theoretical calculations that did not find any Lu-N-H phases with room-temperature superconductivity [45].

The highest T_c compound we found, fluorite-type LuNH ($F\bar{4}3m$), can be derived from LuH_2 by replacing 50% of the hydrogen atoms by nitrogen [Fig. 3(f)]. This chemical substitution dramatically increased the EPC, placing it in the realm of the ambient pressure conventional superconductor with the highest confirmed T_c , MgB_2 . However, the larger λ of 0.78 was attained at a cost of the thermodynamic stability: while $C1$ LuH_2 fell on the 10 kbar hull, LuNH was 564 meV/atom above the hull, suggesting it could never be made. The T_c of LuNH (~ 17 K) was estimated to be a factor of 2 smaller than that of MgB_2 with its strong covalent B-B bonds, whose motions, with frequencies around 600 cm^{-1} , yield an ω_{ln} of 504 cm^{-1} (or 725 K) [90]. As we shall soon see, in LuNH the EPC is relatively evenly distributed from the high-frequency motions of the hydrogen vibrations to the very low-frequency acoustic modes. Their α^2F -weighted logarithmic average yields an ω_{ln} of 257 cm^{-1} (or ~ 370 K). Numerical solution of the Eliashberg equations raised the T_c of LuNH only slightly to ~ 18 K.

It is currently well established that the inclusion of quantum fluctuations and anharmonicity is necessary for a proper description of the phase stability and superconductivity of hydrogen-rich systems. These effects can often lead to structural renormalizations and significant variations in the value of the T_c [91–93]. Additionally, a study performed by Lucrezi *et al.* [94] has shown that in LuH_3 the structure is stabilized by such effects. We used the stochastic self-consistent harmonic approximation (SSCHA) [95] to test the contribution of quantum fluctuations and anharmonicity for the $F\bar{4}3m$ LuNH system. The results reveal no significant variation in the structure or in the value of the T_c . Additional details are reported in the Supplemental Material [55].

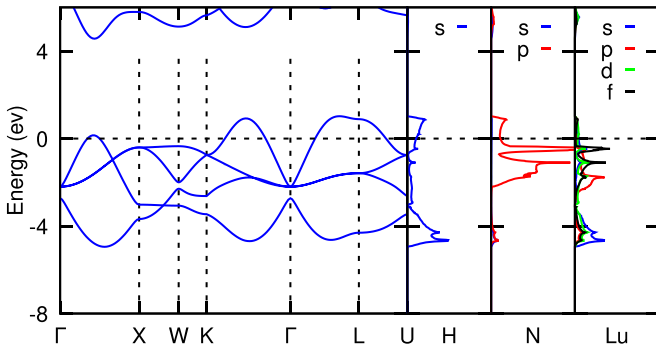


FIG. 7. PBE band structure and projected densities of states of fluorite-type LuNH at 10 kbar.

Let us examine the electronic structure of CaF₂-type LuNH and its contributions to the EPC to better understand how these factors influence the T_c . Replacing H by N in LuH₂ increases the density of states (DOS) at the Fermi level (E_F) by around 50% from 0.019 to 0.027 states/eV/Å³, concomitantly increasing the T_c . As shown in Fig. 7, the major contributions to the DOS at E_F are the H 1s and N 2p states, with a negligible amount from the metal, indicative of a +3 oxidation state. The primitive cell of LuNH contains one formula unit, and as a result its conduction band is half-filled. The reaction $\text{LuNH} + \frac{1}{2}\text{H}_2 \rightarrow \text{LuN} + \text{H}_2$ is exothermic by 400 meV/atom; we would therefore expect the products of this reaction to be found in a CSP search for unit cells whose sizes approach infinity.

Pivoting to the phonon band structure in Fig. 8, we observe that the large differences in the mass between the three elements split their bands nicely into three regions. The vibrational modes of lutetium are mainly below 140 cm⁻¹ (acoustic region), those of nitrogen are between 380 and 470 cm⁻¹, and those of hydrogen are above 660 cm⁻¹. It should be noted that due to the extremely heavy mass of lutetium versus nitrogen and hydrogen (175 versus 14 and 1 a.u.), lutetium moves roughly ten times slower than the hydrogen, and four times slower than the nitrogen. As a result, the atomic displacements of the nitrogen and hydrogen atoms along the low-frequency acoustic modes are still significant.

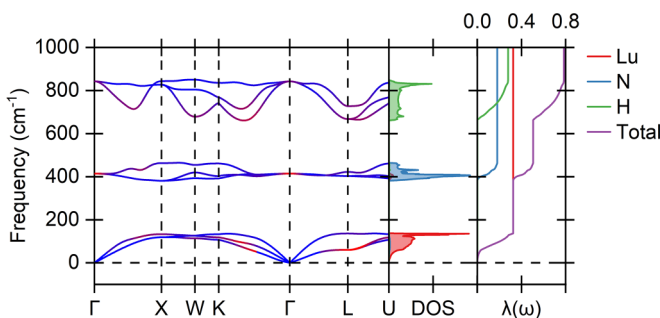


FIG. 8. Phonon dispersion curve and projected EPC constant (λ_{qv}). Blue indicates λ_{qv} approaches 0, and red indicates λ_{qv} approaches the maximum value of 0.36. The atom-projected phonon density of states is illustrated, along with the total λ and the integral of $\lambda(\omega)$ separated into regions comprising the Lu-, N-, and H-based modes.

Because of the separation of these vibrational modes, their contribution to the total EPC can be obtained: motions from the acoustic modes contribute 41%, 23% from the nitrogen-active region, and 35% from the hydrogen-active region. The largest Lu-based contribution originates from the lower two acoustic phonon branches around the middle of the Γ -K path, and also around the L point. Visualization of these motions shows that they result in the formation of N-Lu-H molecular fragments and a hexagonal-like Lu lattice. In the nitrogen-active region, the largest EPC is found at the Γ point, resulting from the nitrogen atoms approaching lutetium to form N-H motifs. In the hydrogen-active region, all of the bands exhibit moderate EPC, especially at several points where the modes are softened; visualization shows that these correspond to the motion of hydrogen atoms closer to lutetium to form H-Lu units.

The ω_{ln} of our Lu-N-H compounds ranged from ~ 150 K ($R3m$ Lu₄NH₄) to 680 K (CaF₂-type LuN_{0.5}H_{1.5}). The absence of high-frequency vibrations in these compounds, resulting from the low pressure and the absence of covalent bonds, suggests that higher ω_{ln} are unlikely to be found in other Lu-N-H compounds at 10 kbar with fcc Lu lattices. Generally speaking, the ω_{ln} calculated for hydrogen and the high- T_c hydrides at extreme pressures is significantly higher, with values of 1200–1800 K not being uncommon. For those hydrides where ω_{ln} values comparable to those we obtain for the Lu-N-H systems have been calculated, room-temperature superconductivity has only been predicted in phases with a very large EPC (e.g., $Fmmm$ ThH₁₈ at 400 GPa, $\omega_{ln} = 568$ K, $\lambda = 3.39$, $T_c = 296$ K) [96]. Therefore, we speculate that similarly very large EPC constants are required for a Lu-N-H compound to be superconducting near room temperature, provided the mechanism is phonon-mediated.

V. CONCLUSIONS

Density functional theory calculations were performed to explore Lu-N-H-containing compounds that could be (meta)stable in a pressure range of about 0–100 kbar (10 GPa). The computations were biased towards systems in which the Lu atoms adopt an fcc arrangement, because it was recently suggested that a compound with this structural feature could be responsible for the near-ambient superconducting critical temperature, T_c , of 294 K reported at 10 kbar [31]. Based on the results of our calculations, we conclude the following:

(i) The Lu-N-H potential energy landscape, within the static lattice approximation and neglecting quantum nuclear and anharmonic effects, contains many local minima with fcc Lu lattices. Other geometries, not explicitly considered here, could be generated via altering the N/H ratio of the solid-solution prototypes we discuss. Which of these structures are synthesizable, and which are kinetically and/or thermally stable and relatively chemically inert, is currently unknown.

(ii) None of the ternary compounds studied here are thermodynamically stable (e.g., they do not lie on the convex hull) up to 10 GPa at 0 K. Only the known binaries—LuH₂, LuH₃, LuN, and NH₃—comprise the convex hull. Thermal effects and the role of configurational entropy on the thermodynamic stability are not known.

(iii) From all of the phases considered here, the one whose equation of states (EOS) had the closest match with the fits to experimental data obtained for compound **A** was fluorite-type LuH_2 , with errors smaller than 0.3% up to 80 kbar. EOS calculations on model compounds suggest that the previously proposed formula for compound **A**, $\text{LuH}_{3-\delta}\text{N}_\epsilon$, would not have the same slope as what was observed experimentally.

(iv) XRD similarity indices for the compounds studied here compared to a pure fcc Lu lattice with the experimental lattice constant indicated a fair match at 0 GPa for binaries LuH_2 , LuH_3 , and ZnS-type LuH, N-substituted ZnS-type LuH, $F\bar{d}3m$ Lu_4NH_7 , and $R3m$ Lu_4NH_4 .

(v) Many, though not all, of the investigated phases exhibited metallic behavior, and their density of states at the Fermi level (DOS at E_F) varied greatly. For example, the main contributions to the DOS at E_F for **B1** and **B3** LuH were the Lu d states; for LuH_2 the DOS at E_F was very small and mainly lutetium p -like, and for LuNH the main components arose from hydrogen s and nitrogen p states.

(vi) The logarithmic average frequency, ω_{ln} , of the Lu-N-H compounds whose superconducting properties were studied ranged from ~ 150 to 680 K, and the electron phonon coupling constants, λ , varied between 0.1 and 0.8. Assuming conventional superconductivity, the T_c s of such compounds can be estimated using the modified McMillan-Allen-Dynes equation. Under this approximation, and with $\mu^* = 0.1$ at 10 kbar, we obtain a T_c of 0.1 K for fluorite LuH_2 . The highest T_c compound we found was fluorite-type LuNH with a T_c of 17 K.

Though we have not uncovered an Lu-N-H-containing phase with a superconducting critical temperature near what

was recently reported in Ref. [31], we believe our computations shed light on the structures that contain these elemental combinations at mild pressures. Future work will ascertain if our choice of standard DFT parameters (gradient-corrected exchange functional, neglect of spin polarization and strong electron correlations, and inclusion of f electrons in the core) impacts our conclusions. Our work also highlights the complexity inherent in the computational search for phases that may be metastable with desired structural and property characteristics in multielement *ab initio* (or even machine-learning-assisted) crystal structure prediction.

Note added. Only a few days after our manuscript was posted on the arXiv, Ferreira *et al.* posted a computational study that used a different strategy to search for candidate stable and metastable Lu-N-H compounds, yet they came to very similar conclusions regarding the potential for superconductivity in these systems at low pressures [97].

ACKNOWLEDGMENTS

We are grateful to R. Dias for sharing experimental data, as well as G. W. Collins and R. J. Hemley for useful discussions. K.H. acknowledges the Chicago/DOE Alliance Center under Cooperative Agreement Grant No. DE-NA0003975, N.G. the U.S. National Science Foundation (DMR-2132491), and F.B. the U.S. National Science Foundation (DMR-2136038) for financial support. This material is based upon work supported by the U.S. Department of Energy, Office of Science, Fusion Energy Sciences funding the award entitled High Energy Density Quantum Matter under Award No. DE-SC0020340. Computations were carried out at the Center for Computational Research at the University at Buffalo [98].

-
- [1] H. K. Onnes, Proc. K. Ned. Akad. Wet. B **14**, 113 (1911).
- [2] M. K. Wu, J. R. Ashburn, C. J. Torng, P. H. Hor, R. L. Meng, L. Gao, Z. J. Huang, Y. Q. Wang, and C. W. Chu, Phys. Rev. Lett. **58**, 908 (1987).
- [3] Z. Z. Sheng and A. M. Hermann, Nature (London) **332**, 138 (1988).
- [4] A. P. Drozdov, M. I. Erements, I. A. Troyan, V. Ksenofontov, and S. I. Shylin, Nature (London) **525**, 73 (2015).
- [5] I. Osmond, O. Moulding, S. Cross, T. Muramatsu, A. Brooks, O. Lord, T. Fedotenko, J. Buhot, and S. Friedemann, Phys. Rev. B **105**, L220502 (2022).
- [6] V. S. Minkov, V. B. Prakapenka, E. Greenberg, and M. I. Erements, Angew. Chem. Int. Ed. **59**, 18970 (2020).
- [7] N. W. Ashcroft, Phys. Rev. Lett. **92**, 187002 (2004).
- [8] K. P. Hilleke and E. Zurek, J. Appl. Phys. **131**, 070901 (2022).
- [9] K. P. Hilleke, T. Bi, and E. Zurek, Appl. Phys. A **128**, 441 (2022).
- [10] E. Zurek and T. Bi, J. Chem. Phys. **150**, 050901 (2019).
- [11] L. Ma, K. Wang, Y. Xie, X. Yang, Y. Wang, M. Zhou, H. Liu, X. Yu, Y. Zhao, H. Wang, G. Liu, and Y. Ma, Phys. Rev. Lett. **128**, 167001 (2022); **129**, 269901(E) (2022).
- [12] Z. Li, X. He, C. Zhang, X. Wang, S. Zhang, Y. Jia, S. Feng, K. Lu, J. Zhao, J. Zhang, B. Min, Y. Long, R. Yu, L. Wang, M. Ye, Z. Zhang, V. Prakapenka, S. Chariton, P. A. Ginsberg, J. Bass, S. Yuan *et al.*, Nat. Commun. **13**, 2863 (2022).
- [13] M. Somayazulu, M. Ahart, A. K. Mishra, Z. M. Geballe, M. Baldini, Y. Meng, V. V. Struzhkin, and R. J. Hemley, Phys. Rev. Lett. **122**, 027001 (2019).
- [14] A. P. Drozdov, P. P. Kong, V. S. Minkov, S. P. Besedin, M. A. Kuzovnikov, S. Mozaffari, L. Balicas, F. F. Balakirev, D. E. Graf, V. B. Prakapenka, E. Greenberg, D. A. Knyazev, M. Tkacz, and M. I. Erements, Nature (London) **569**, 528 (2019).
- [15] E. Snider, N. Dasenbrock-Gammon, R. McBride, X. Wang, N. Meyers, K. V. Lawler, E. Zurek, A. Salamat, and R. P. Dias, Phys. Rev. Lett. **126**, 117003 (2021).
- [16] I. A. Troyan, D. V. Semenok, A. G. Kvashnin, A. V. Sadakov, O. A. Sobolevskiy, V. M. Pudalov, A. G. Ivanova, V. B. Prakapenka, E. Greenberg, A. G. Gavriliuk, I. S. Lyubutin, V. V. Struzhkin, A. Bergara, I. Errea, R. Bianco, M. Calandra, F. Mauri, L. Monacelli, R. Akashi, and A. R. Oganov, Adv. Mater. **33**, 2006832 (2021).
- [17] D. V. Semenok, I. A. Troyan, A. G. Ivanova, A. G. Kvashnin, I. A. Kruglov, M. Hanfland, A. V. Sadakov, O. A. Sobolevskiy, K. S. Pervakov, I. S. Lyubutin, K. V. Glazyrin, N. Giordano, D. N. Karimov, A. L. Vasiliev, R. Akashi, V. M. Pudalov, and A. R. Oganov, Mater. Today **48**, 18 (2021).
- [18] P. Song, Z. Hou, P. Baptista de Castro, K. Nakano, K. Hongo, Y. Takano, and R. Maezono, Chem. Mater. **33**, 9501 (2021).

- [19] D. V. Semenov, I. A. Kruglov, I. A. Savkin, A. G. Kvashnin, and A. R. Oganov, *Curr. Opin. Solid State Mater. Sci.* **24**, 100808 (2020).
- [20] F. Peng, Y. Sun, C. J. Pickard, R. J. Needs, Q. Wu, and Y. Ma, *Phys. Rev. Lett.* **119**, 107001 (2017).
- [21] W. Sun, X. Kuang, H. D. J. Keen, C. Lu, and A. Hermann, *Phys. Rev. B* **102**, 144524 (2020).
- [22] H. Song, Z. Zhang, T. Cui, C. J. Pickard, V. Z. Kresin, and D. Duan, *Chin. Phys. Lett.* **38**, 107401 (2021).
- [23] Z. Li, X. He, C. Zhang, K. Lu, B. Min, J. Zhang, S. Zhang, J. Zhao, L. Shi, Y. Peng, S. Feng, Z. Deng, J. Song, Q. Liu, X. Wang, R. Yu, L. Wang, Y. Li, J. D. Bass, V. Prakapenka, S. Chariton, H. Liu, and C. Jin, *Sci. China: Phys. Mech. Astron.* **66**, 267411 (2023).
- [24] D. Laniel, F. Trybel, B. Winkler, F. Knoop, T. Fedotenko, S. Khandarkhaeva, A. Aslandukova, T. Meier, S. Chariton, K. Glazyrin, V. Milman, V. Prakapenka, I. A. Abrikosov, L. Dubrovinsky, and N. Dubrovinskaja, *Nat. Commun.* **13**, 6987 (2022).
- [25] M. Peña-Alvarez, J. Binns, M. Martinez-Canales, B. Monserrat, G. J. Ackland, P. Dalladay-Simpson, R. T. Howie, C. J. Pickard, and E. Gregoryanz, *J. Phys. Chem. Lett.* **12**, 4910 (2021).
- [26] D. V. Semenov, D. Zhou, A. G. Kvashnin, X. Huang, M. Galasso, I. A. Kruglov, A. G. Ivanova, A. G. Gavriliuk, W. Chen, N. V. Tkachenko, A. I. Boldyrev, I. Troyan, A. R. Oganov, and T. Cui, *J. Phys. Chem. Lett.* **12**, 32 (2021).
- [27] S. Di Cataldo, C. Heil, W. von der Linden, and L. Boeri, *Phys. Rev. B* **104**, L020511 (2021).
- [28] A. P. Durajski and R. Szcześniak, *Phys. Chem. Chem. Phys.* **23**, 25070 (2021).
- [29] Y. Zhao, X. Zhang, X. Li, S. Ding, Y. Liu, and G. Yang, *J. Mater. Chem. C* **10**, 14626 (2022).
- [30] N. Geng, K. P. Hilleke, L. Zhu, X. Wang, T. A. Strobel, and E. Zurek, *J. Am. Chem. Soc.* **145**, 1696 (2023).
- [31] N. Dasenbrock-Gammon, E. Snider, R. McBride, H. Pasan, D. Durkee, N. Khalvashi-Sutter, S. Munasinghe, S. E. Dissanayake, K. V. Lawler, A. Salamat, and R. P. Dias, *Nature (London)* **615**, 244 (2023).
- [32] L. Deng, T. Bontke, R. Dahal, Y. Xie, B. Gao, X. Li, K. Yin, M. Gooch, D. Rolston, T. Chen, Z. Wu, Y. Ma, P. Dai, and C. Chu, *Proc. Natl. Acad. Sci. USA* **118**, e21089381138 (2021).
- [33] P. Shan, N. Wang, X. Zheng, Q. Qiu, Y. Peng, and J. Cheng, *Chinese Phys. Lett.* **40**, 046101 (2023).
- [34] X. Ming, Y.-J. Zhang, X. Zhu, Q. Li, C. He, Y. Liu, T. Huang, G. Liu, B. Zheng, H. Yang *et al.*, *Nature (London)* (2023), doi: 10.1038/s41586-023-06162-w.
- [35] X. Zhao, P. Shan, N. Wang, Y. Li, Y. Xu, and J. Cheng, *Sci. Bull.* **68**, 883 (2023).
- [36] Y.-J. Zhang, X. Ming, Q. Li, X. Zhu, B. Zheng, Y. Liu, C. He, H. Yang, and H.-H. Wen, *Sci. China Phys. Mech. Astron.* **66**, 287411 (2023).
- [37] X. Xing, C. Wang, L. Yu, J. Xu, C. Zhang, M. Zhang, S. Huang, X. Zhang, B. Yang, X. Chen, Y. Zhang, J. Guo, Z. Shi, Y. Ma, C. Chen, and X. Liu, [arXiv:2303.17587](https://arxiv.org/abs/2303.17587).
- [38] O. Moulding, S. Gallego-Parra, P. Toulemonde, G. Garbarino, P. Derango, P. Giroux, and M.-A. Measson, [arXiv:2304.04310](https://arxiv.org/abs/2304.04310).
- [39] N. Wang, J. Hou, Z. Liu, P. Shan, C. Chai, S. Jin, X. Wang, Y. Long, Y. Liu, H. Zhang *et al.*, [arXiv:2304.00558](https://arxiv.org/abs/2304.00558).
- [40] S. Cai, J. Guo, H. Shu, L. Yang, P. Wang, Y. Zhou, J. Zhao, J. Han, Q. Wu, W. Yang *et al.*, *Matter Radiat. Extremes* **8**, 048001 (2023).
- [41] S. Zhang, J. Bi, R. Zhang, P. Li, F. Qi, Z. Wei, and Y. Cao, *AIP Adv.* **13**, 065117 (2023).
- [42] M. Liu, X. Liu, J. Li, J. Liu, Y. Sun, X.-Q. Chen, and P. Liu, *Phys. Rev. B* **108**, L020102 (2023).
- [43] F. Xie, T. Lu, Z. Yu, Y. Wang, Z. Wang, S. Meng, and M. Liu, *Chinese Phys. Lett.* **40**, 057401 (2023).
- [44] Y. Sun, F. Zhang, S. Wu, V. Antropov, and K.-M. Ho, *Phys. Rev. B* **108**, L020101 (2023).
- [45] Z. Huo, D. Duan, T. Ma, Z. Zhang, Q. Jiang, D. An, H. Song, F. Tian, and T. Cui, *Matter Radiat. Extremes* **8**, 038402 (2023).
- [46] T. Lu, S. Meng, and M. Liu, [arXiv:2304.06726](https://arxiv.org/abs/2304.06726).
- [47] Đ. Dangić, P. Garcia-Goiricelaya, Y.-W. Fang, J. Ibañez-Azpiroz, and I. Errea, [arXiv:2305.06751](https://arxiv.org/abs/2305.06751).
- [48] S.-W. Kim, L. J. Conway, C. J. Pickard, G. L. Pascut, and B. Monserrat, [arXiv:2304.07326](https://arxiv.org/abs/2304.07326).
- [49] J. E. Hirsch, *J. Supercond. Nov. Magn.* **615**, 244 (2023).
- [50] J. P. Perdew, K. Burke, and M. Ernzerhof, *Phys. Rev. Lett.* **77**, 3865 (1996).
- [51] G. Kresse and J. Furthmüller, *Comput. Mater. Sci.* **6**, 15 (1996).
- [52] G. Kresse and J. Furthmüller, *Phys. Rev. B* **54**, 11169 (1996).
- [53] G. Kresse and D. Joubert, *Phys. Rev. B* **59**, 1758 (1999).
- [54] P. E. Blöchl, *Phys. Rev. B* **50**, 17953 (1994).
- [55] See Supplemental Material at <http://link.aps.org/supplemental/10.1103/PhysRevB.108.014511> for the results of detailed tests of the inclusion of the 4f electrons on the properties of select structures, detailed structural information, electronic and phonon band structures, and additional information regarding calculation of quantum anharmonic effects.
- [56] H. J. Monkhorst and J. D. Pack, *Phys. Rev. B* **13**, 5188 (1976).
- [57] A. Togo and I. Tanaka, *Scr. Mater.* **108**, 1 (2015).
- [58] A. Togo, *J. Phys. Soc. Jpn.* **92**, 012001 (2023).
- [59] E. Plekhanov, Z. Zhao, F. Macheda, Y. Wei, N. Bonini, and C. Weber, *Phys. Rev. Res.* **4**, 013248 (2022).
- [60] P. Giannozzi, S. Baroni, N. Bonini, M. Calandra, R. Car, C. Cavazzoni, D. Ceresoli, G. L. Chiarotti, M. Cococcioni, I. Dabo, A. D. Corso, S. de Gironcoli, S. Fabris, G. Fratesi, R. Gebauer, U. Gerstmann, C. Gougoussis, A. Kokalj, M. Lazzeri, L. Martin-Samos *et al.*, and *J. Phys.: Condens. Matter* **21**, 395502 (2009).
- [61] P. Giannozzi Jr, O. Andreussi, T. Brumme, O. Bunau, M. B. Nardelli, M. Calandra, R. Car, C. Cavazzoni, D. Ceresoli, M. Cococcioni, N. Colonna, I. Carnimeo, A. D. Corso, S. de Gironcoli, P. Delugas, R. A. DiStasio, A. Ferretti, A. Floris, G. Fratesi, G. Fugallo *et al.*, *J. Phys.: Condens. Matter* **29**, 465901 (2017).
- [62] A. Dal Corso, *Comput. Mater. Sci.* **95**, 337 (2014).
- [63] P. B. Allen and R. C. Dynes, *Phys. Rev. B* **12**, 905 (1975).
- [64] G. Eliashberg, *Sov. Phys. JETP* **11**, 696 (1960).
- [65] D. C. Lonie and E. Zurek, *Comput. Phys. Commun.* **182**, 372 (2011).
- [66] [http://xtalopt.github.io/](https://xtalopt.github.io/).
- [67] Z. Falls, P. Avery, X. Wang, K. P. Hilleke, and E. Zurek, *J. Phys. Chem. C* **125**, 1601 (2021).
- [68] P. Avery, C. Toher, S. Curtarolo, and E. Zurek, *Comput. Phys. Commun.* **237**, 274 (2019).

- [69] P. Avery and E. Zurek, *Comput. Phys. Commun.* **213**, 208 (2017).
- [70] D. C. Lonie and E. Zurek, *Comput. Phys. Commun.* **183**, 690 (2012).
- [71] S. P. Ong, W. D. Richards, A. Jain, G. Hautier, M. Kocher, S. Cholia, D. Gunter, V. L. Chevrier, K. A. Persson, and G. Ceder, *Comput. Mater. Sci.* **68**, 314 (2013).
- [72] B. Wang, K. P. Hilleke, S. Hajinazar, G. Frapper, and E. Zurek, [arXiv:2306.01873](https://arxiv.org/abs/2306.01873).
- [73] S. K. Singh and U. Verma, *J. Phys.: Conf. Ser.* **640**, 012029 (2015).
- [74] G. G. Libowitz, *Ber. Bunseng. Physik. Chem.* **76**, 837 (1972).
- [75] R. Kataoka, T. Kojima, K. Tada, M. Kitta, N. Takeichi, K. Sakaki, M. Nozaki, T. Kimura, and A. Kamegawa, *Materialia* **15**, 100956 (2021).
- [76] M. Shao, S. Chen, W. Chen, K. Zhang, X. Huang, and T. Cui, *Inorg. Chem.* **60**, 15330 (2021).
- [77] A. Pebler and W. Wallace, *J. Phys. Chem.* **66**, 148 (1962).
- [78] G. L. Olcese, *J. Phys. F: Met. Phys.* **9**, 569 (1979).
- [79] L.-g. Liu, *J. Phys. Chem. Solids* **36**, 31 (1975).
- [80] F. H. Spedding, J. J. Hanak, and A. H. Daane, *J. Less-Common Met.* **3**, 110 (1961).
- [81] C. J. Pickard and R. J. Needs, *Nat. Phys.* **3**, 473 (2007).
- [82] J. Donohue, *Acta Crystallogr.* **14**, 1000 (1961).
- [83] R. L. Mills, B. Olinger, and D. T. Cromer, *J. Chem. Phys.* **84**, 2837 (1986).
- [84] C. J. Pickard and R. Needs, *Nat. Mater.* **7**, 775 (2008).
- [85] W. Sun, S. T. Dacek, S. P. Ong, G. Hautier, A. Jain, W. D. Richards, A. C. Gamst, K. A. Persson, and G. Ceder, *Sci. Adv.* **2**, e1600225 (2016).
- [86] K. Yang, C. Oses, and S. Curtarolo, *Chem. Mater.* **28**, 6484 (2016).
- [87] J. Gonzalez-Platas, M. Alvaro, and F. Nestola, *R. Angel. Appl. Crystallogr.* **49**, 1377 (2016).
- [88] S. Fredericks, K. Parrish, D. Sayre, and Q. Zhu, *Comput. Phys. Commun.* **261**, 107810 (2021).
- [89] J. Wittig, C. Probst, and W. Wiedemann, in *Low Temperature Physics-LT 13*, edited by K. D. Timmerbaas, W. J. O'Sullivan, E. F. Hammel, Volume 3: Superconductivity (Springer, New York, 1974), p. 490.
- [90] Y. Kong, O. V. Dolgov, O. Jepsen, and O. K. Andersen, *Phys. Rev. B* **64**, 020501(R) (2001).
- [91] I. Errea, M. Calandra, C. J. Pickard, J. R. Nelson, R. J. Needs, Y. Li, H. Liu, Y. Zhang, Y. Ma, and F. Mauri, *Nature (London)* **532**, 81 (2016).
- [92] I. Errea, F. Belli, L. Monacelli, A. Sanna, T. Koretsune, T. Tadano, R. Bianco, M. Calandra, R. Arita, F. Mauri *et al.*, *Nature (London)* **578**, 66 (2020).
- [93] F. Belli and I. Errea, *Phys. Rev. B* **106**, 134509 (2022).
- [94] R. Lucrezi, P. P. Ferreira, M. Aichhorn, and C. Heil, [arXiv:2304.06685](https://arxiv.org/abs/2304.06685).
- [95] L. Monacelli, R. Bianco, M. Cherubini, M. Calandra, I. Errea, and F. Mauri, *J. Phys.: Condens. Matter* **33**, 363001 (2021).
- [96] X. Zhong, Y. Sun, T. Iitaka, M. Xu, H. Liu, R. J. Hemley, C. Chen, and Y. Ma, *J. Am. Chem. Soc.* **144**, 13394 (2022).
- [97] P. P. Ferreira, L. J. Conway, A. Cucciari, S. Di Cataldo, F. Giannessi, E. Kogler, L. T. F. Eleno, C. J. Pickard, C. Heil, and L. Boeri, [arXiv:2304.04447](https://arxiv.org/abs/2304.04447).
- [98] <http://hdl.handle.net/10477/79221>.